From {Au^I···Au^I}-Coupled Cages to the Cage-Built 2-D {Au^I···Au^I} Arrays: Au^I···Au^I Bonding Interaction Driven Self-Assembly and Their Ag^I Sensing and Photo-Switchable Behavior

Xuan-Feng Jiang,[†] Franky Ka-Wah Hau,[‡] Qing-Fu Sun,[∥] Shu-Yan Yu,*[,†,§] and Vivian Wing-Wah Yam*[,‡]

[†]Beijing Key Laboratory for Green Catalysis and Separation, Department of Chemistry and Chemical Industry, College of Environmental and Energy Engineering, Beijing University of Technology, Beijing 100124, P. R. China

[‡]Institute of Molecular Functional Materials (Areas of Excellence Scheme, University Grants Committee (Hong Kong)) and Department of Chemistry, The University of Hong Kong, Pokfulam Road, Hong Kong, P. R. China

[§]Laboratory for Self-Assembly Chemistry, Department of Chemistry, Renmin University of China, Beijing 100872, P. R. China

[∥]State Key Laboratory of Structural Chemistry, Fujian Institute of Research on the Structure of Matter, Chinese Academy of Sciences, Fuzhou 350002, P.R. China

S *Supporting Information*

ABSTRACT: Metal−metal bonding interactions have been used to generate a number of unique supramolecular assemblies with fascinating functions. We presented here a new class of gold(I)-containing metallosupramolecular cages and cage-built two-dimensional (2-D) arrays of {Au$_8$L$_2$}$_n$ (n = 1 or ∞, L = tetrakis-dithiocarbamato-calix[4]arene, TDCC), **1−3**, which are constructed from the self-assembly of deep-cavitand calix[4]arene-based supramolecular cages consisting of octanuclear Au(I) motifs. Synchrotron radiation X-ray diffraction structural analyses of **1−3** revealed their quadruple-stranded helicate dimeric cage structure and the presence of 2-D arrays of cages linked together by inter- and intramolecular Au^I···Au^I interactions. Electronic absorption and emission studies of complexes **1−3** indicated the occurrence of a programmable self-assembly process in a concentration-dependent stepwise manner with the links built via aurophilic interactions. These novel gold(I) supramolecular cages exhibited green phosphorescence and have been shown to serve as highly selective proof-of-concept luminescent sensors toward Ag^I cation among various competitive transition-metal ions.

Capsule [Au$_8$L$_2$]   Ag$^+$ / I$^-$ [Au$_8$L$_2$] · Ag$^+$
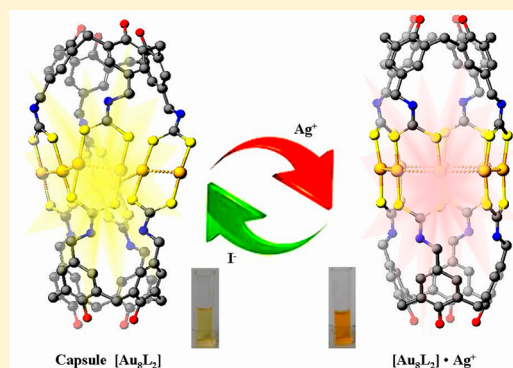
INTRODUCTION

Over the past decades, the study of polynuclear gold(I) complexes, in particular, with regard to the phenomenon of aurophilicity, has attracted increasing attention.[1−15] At the same time, the self-assembly approaches have become a powerful strategy for the construction of various supramolecular systems.[16−18] Covalent bonds, hydrogen bonds, and metal coordination bonds play crucial roles in the controlled constructions of well-defined nanoscale supramolecular aggregates.[16−18] Recently, inter- or intramolecular Au^I···Au^I bonding interactions, which have similar strengths as hydrogen bonds, have emerged as a new structural motif in the design and construction of supramolecular aggregates.[3,7−15] Among the various systems, the self-assembly of homo- and heteronuclear gold(I) complexes with metal−metal interactions or bonds continues to attract immense attention not only because of their structural diversity such as discrete dimers and complexes,[9] polynuclear macrocycles,[10,11] cages,[15c] polyhedron clusters,[4] catenanes,[15a,b] extended molecular atom chains[13,14] and polymers[12] but also due to their wide and potential applications as chemical sensors,[9d,e,11d] optoelectronic materi-

als,[17e,f] molecular machines and devices,[17g] gelators,[13a] vapochromic materials[14] and others. Owing to their fascinating photophysical and electrochemical properties, there has been a growing interest in the design and construction of many novel aggregates through the utilization of polyfunctional building units to achieve efficient self-assembly via aurophilic interactions. Therefore, the utilization of multiple metal coordination and metal−metal bonding interactions has extended such chemistry toward the emerging area of large metallo-organic assemblies in supramolecular gold chemistry. Using a Au^I···Au^I bonding interaction-directed stepwise macrocyclization strategy, our group has developed a series of giant ring systems from Au$_{12}$ to Au$_{16}$, Au$_{18}$, and Au$_{36}$ with novel luminescence properties in some cases.[11]

We herein report a new class of gold(I)-containing metallosupramolecular cages {Au$_8$L$_2$} (L = tetrakis-dithiocarbamato-calix[4]arene, TDCC), **1−3**, which are self-assembled from two deep-cavitand calix[4]arene-based dithiocarbamate

Scheme 1. Self-Assembly Pathway With the 3-D Supramolecular Cages As the Building Units[a]
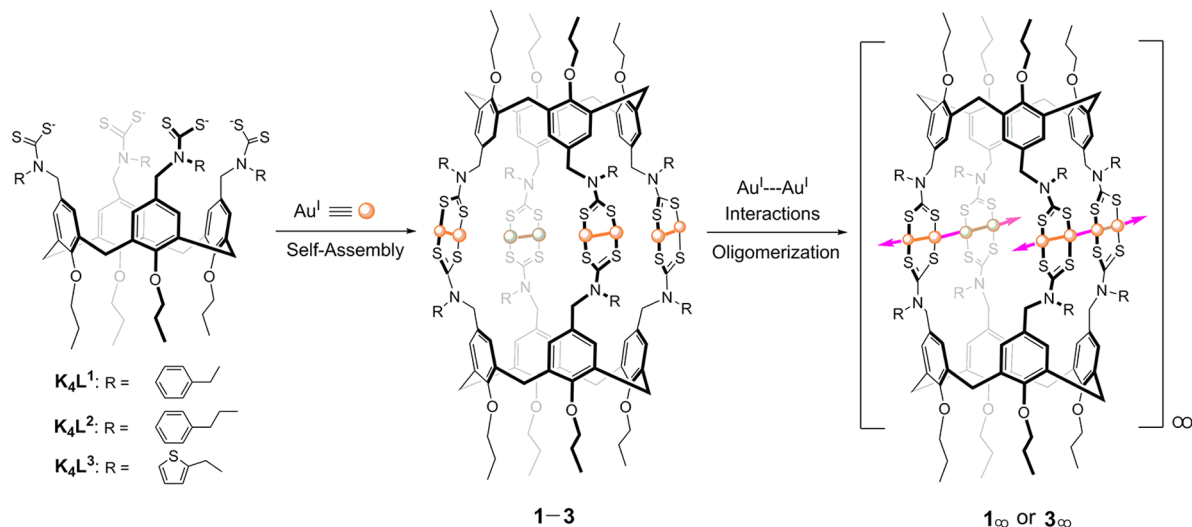
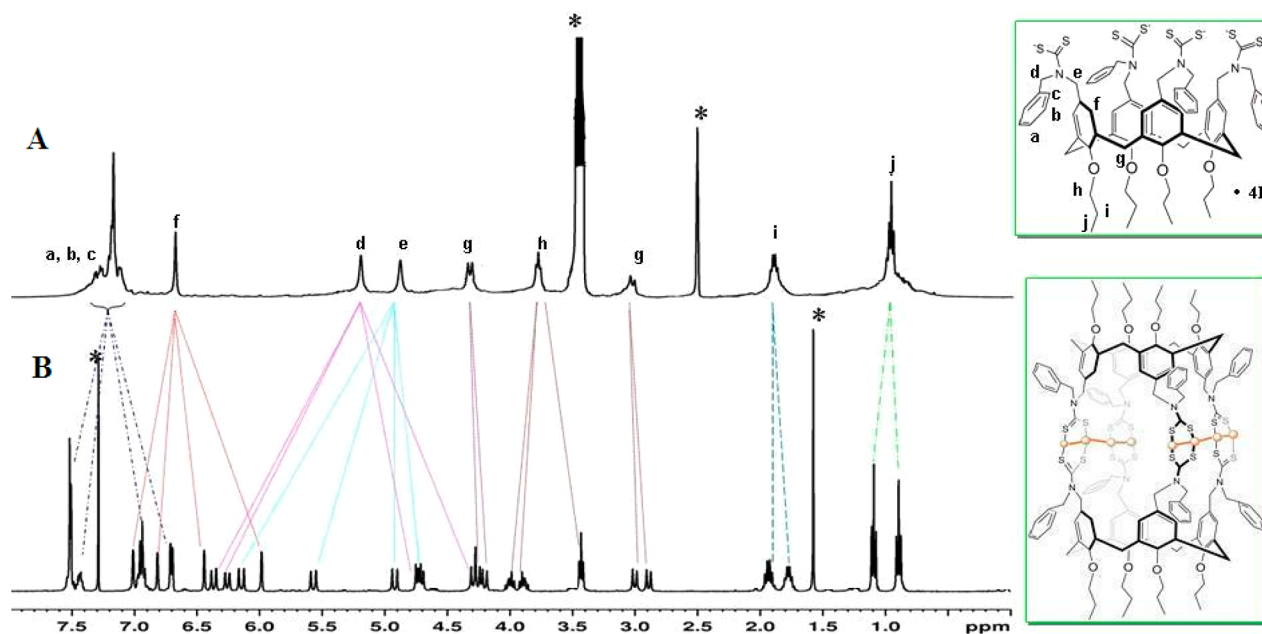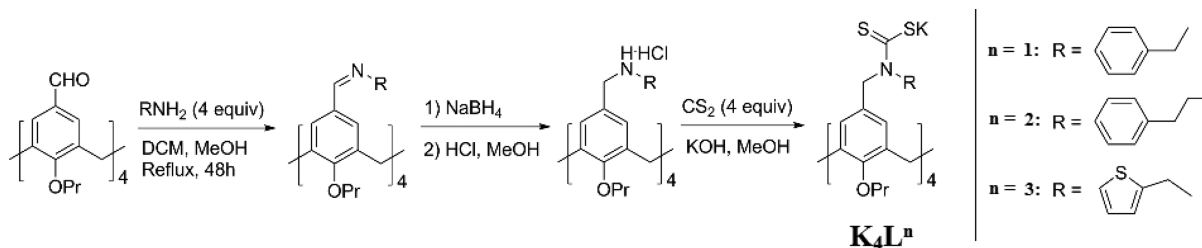^{a} L = tetrakis-dithiocarbamato-calix[4]arene cavitands, TDCC.

Scheme 2. Synthetic Routes of Tetrakis(dithiocarbamato)-tetrapropoxycalix[4]arene Ligands K_4L^n ($n = 1-3$)

Figure 1. ^{1}H NMR spectra of ligand K_4L^1 and complex **1** in CDCl$_3$ with dashed lines showing the symmetry change before and after the complexation. (A) Free dithiocarbamate ligand K_4L^1; (B) [Au$_8$L$^1_2$] chiral capsule **1**. (Lower-case letters represent corresponding protons from calix[4]arene ligand: a−c, Ar-phenylmethyl; d and e, -NR-; f, Ar-(calix); g, ArCH$_2$Ar; h−j, propoxy. The signals of solvents are labeled with*).

ligands and eight Au(I) metal centers featuring a quadruple-stranded helicate structure. Interestingly, these functional supramolecular metallo-organic cages aggregate into two-dimensional sheet-like molecular arrays in the solid state,

consisting of one-dimensional molecular wires with extended intra- and intermolecular Au^I···Au^I bonding interactions (Scheme 1). The electronic absorption and emission spectra of complexes **1−3** confirm that the programmable self-assembly
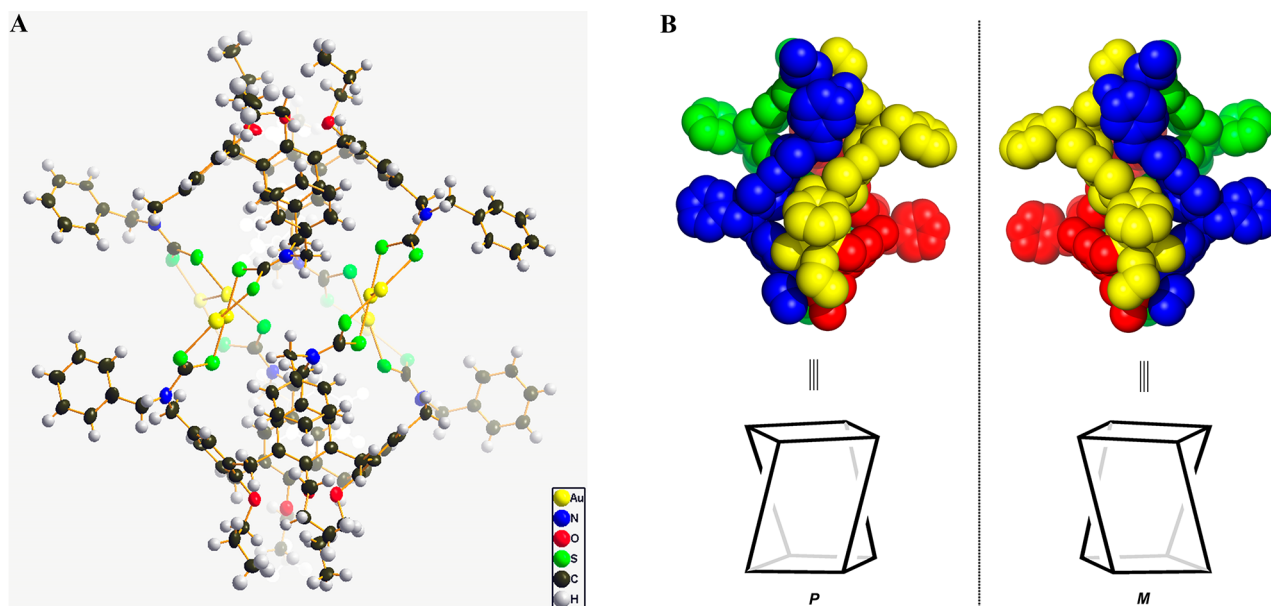
Figure 2. (A) Perspective view for the crystal structure of **1** with thermal ellipsoids shown at 50% probability level. (B) Two enantiomeric quadruple-stranded structure of **1** with cartoon representation for both the *P* and *M* helicity.

process occurs in a stepwise manner with the links built via aurophilic interactions. Photophysical investigations in the solution state revealed that the gold(I) molecular capsules could function as highly selective proof-of-concept phosphorescent sensors for silver ions and reversible light-convertible ion switches. Such supramolecular assemblies exhibit potential applications in host–guest chemistry, molecular recognition, and may serve as selective luminescent materials for sensors and OLEDs.

■ RESULTS AND DISCUSSION

The General Preparation and Characterization of Ligands and Gold(I) Complexes 1−3. Tetrakis-dithiocarbamato-calix[4]arene (TDCC) ligands, K_4L (L = L^1, L^2, L^3), were prepared via multistep reactions in good yield (70−80%) by using synthetic approaches similar to those reported previously.[11,18] All the reactions were carried out under an inert atmosphere of argon (Scheme 2). Addition of [Au(tht)-Cl] (tht = tetrahydrothiophene) in dichloromethane to a suspension of 0.25 mol equiv of ligand K_4L in ethanol at room temperature for 24 h (Scheme 2) resulted in the formation of a yellow precipitate. After evaporation of the solvent from the reaction mixture under vacuum, the residue was purified by flash chromatography on silica gel with hexane-CH_2Cl_2 as eluent. Slow diffusion of diethyl ether into the concentrated yellow solution at room temperature gave **1** as diffraction-quality red block crystals. The structure was subsequently confirmed by X-ray crystallography (Figure 2). The same synthetic procedures were employed to produce cage **2** and **3** also as block crystals.

The ^1H NMR spectrum revealed that a change of symmetry from C_{4v} of the free ligand K_4L^1 to D_2 of cage **1** occurred after complexation with Au^I metal centers. As shown in Figure 1, it is remarkable to note that the only singlet of the aryl protons on the calix[4]arene unit is split into four singlet signals. While the free ligand (K_4L^1) bears a C_{4v} symmetry with proton resonances of the propoxy substituents on the periphery of the calix[4]arene in K_4L^1 appearing as three signals at δ 1.0, 1.9,

and 3.8 ppm, the propoxy signals at δ 1.0 and 1.9 ppm are split into four sets of multiplets and the propoxy signals near the oxygen at δ 3.8 ppm are split into one set of triplet signals at δ 3.97 ppm and two sets of multiplet signals at δ 3.41 and 3.86 ppm in cage **1** after complexation. Similar to the changes described above, the methylene protons (-ArCH_2Ar-) on the rim of the calix[4]arene are split from two sets into four sets of signals found at δ 2.87, 3.02, 4.21, and 4.28 ppm.[18e,f] The other two methylene groups near the nitrogen atom (-CH_2NCH_2-) are also split from two singlets into four pairs of doublets, respectively. These are in line with the diastereotopic relationships of the methylene protons in the propoxy groups arising from the chirality and the orientation of the -NR- groups due to restricted geometrical constraints in the molecules. When the ^1H NMR spectra of cage **1** at different concentrations in the range of 0.42 to 4.17 mM are examined (Figure S31), the NMR spectra and the chemical shifts were found to be not much affected by a change in the concentration. Furthermore, temperature-dependent ^1H NMR spectra also revealed that the twisted chiral conformation remained essentially intact upon a change of temperature between 298 and 353 K (Figure S32). The $^1H−^1H$ COSY spectra further confirmed these splitting patterns with clear cross peaks between the pairs (Figures S28 and S29). These findings suggested the chiral structure of the product, which has been confirmed by X-ray crystal structure determination (see Structure Determination section below), that remained intact in solution. MALDI-TOF-MS gave a formula of **1** as $Au_8L^1_2$ with signals found at m/z = 3914.5, 4115.5, 4312, corresponding to the fragments of $[Au_6L^1_2]^+$, $[Au_7L^1_2]^+$, and $[Au_8L^1_2]^+$ cluster ions, respectively (Figure S33). Likewise, the combination of ligands K_4L^2 and K_4L^3 with [Au(tht)Cl] in CH_3OH solution gave rise to the formation of **2** and **3** correspondingly, which have been fully characterized by ^1H NMR spectroscopy, MALDI-TOF-MS and X-ray crystal structure determination.

10923

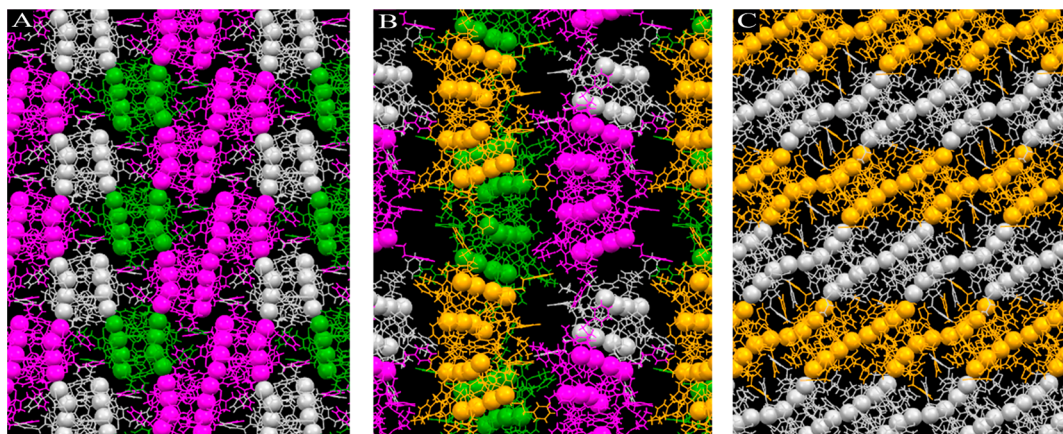dx.doi.org/10.1021/ja502295c | *J. Am. Chem. Soc.* 2014, 136, 10921−10929

Figure 3. Packing of a single-layer 2-D molecular arrays in the crystal structure of cages **1** (A), **2** (B), and **3** (C) viewing along the *c*, *a*, and *a* axes, respectively. The cage units are shown in different colors defined by symmetry operations. To highlight their differences in the intercage Au^I···Au^I interactions, Au atoms are drawn in the spacefill and all the other atoms in the wireframe styles, respectively.
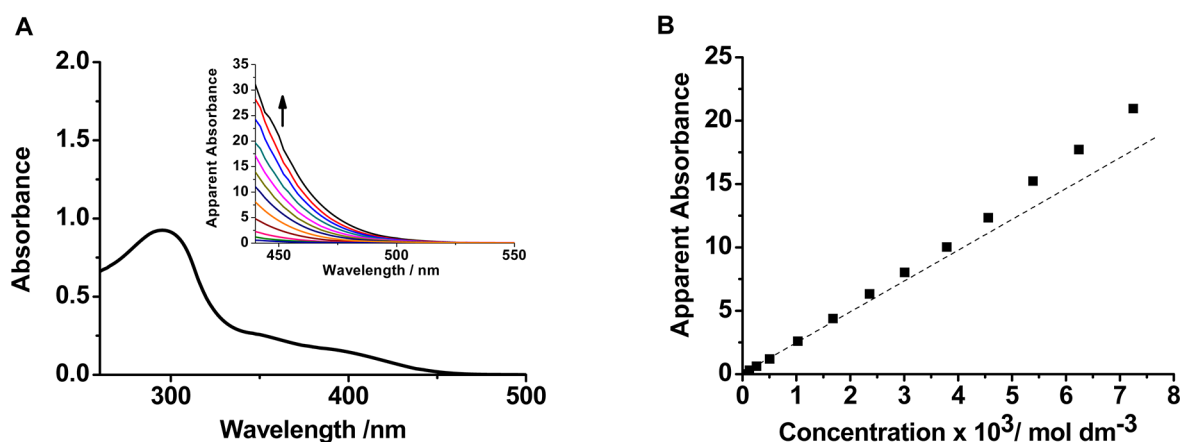

Figure 4. (A) UV−Vis absorption spectrum of complex **1** in dichloromethane. Inset: UV−Vis absorption spectral changes of complex **1** in dichloromethane as the concentration increases from 1.32×10^{-4} to 7.25×10^{-3} M. The apparent absorbance values have been corrected to a 1 cm path-length equivalence. (B) A plot of absorbance at 450 nm as a function of concentration for complex **1**. Experimental (■) and theoretical (---) fit to Beer's law.

■ STRUCTURE DETERMINATION

Single crystals of cage **1** were obtained by a slow vapor diffusion of diethyl ether into a methylene chloride solution of the complex; the structure of which has been unambiguously confirmed by synchrotron radiation X-ray crystallography. Cage **1** crystallizes in an orthorhombic *Aba*2 space group, with noncentrosymmetry and a 2-fold screw axis (Figure 2A). The flexible polydentate bridging dithiocarbamate ligands functionalized on the upper rim of the bowl-shaped calix[4]arene have been employed to coordinate to four sets of dinuclear gold(I) units to form a 3-D cage, {Au$_8$L$_2$}. In the metal−organic gold(I)-centered cage-like structure of **1**, the freely tunable calix[4]arene-based cavitands mainly adopt a favorable 1,3-expanded and 2,4-contracted conformation to meet the steric demand, leading to the formation of a quadruple-stranded helicate structure (Figure 2B). It is worthy to note that two types of Au^I···Au^I interactions with different strengths exist in the cage. While interactions are observed as expected inside the dinuclear Au^I units with an average Au···Au distance of 2.78 Å, two weaker interactions are also observed between the neighboring two dinuclear Au^I units with an average bond distance of 2.95 Å. The latter interaction may help to hold the chiral helicate conformation. Formation of supramolecular

chirality from achiral building units has been reported previously in the Au$_{16}$ and Au$_{12}$ ring-like cluster systems by our group.[11a,c] Crystal structures of complexes **2** and **3** have also been obtained and all show a similar quadruple-stranded helicate structure as **1**.[19] Cage **2** crystallizes in monoclinic $P2_1/n$ space group, while cage **3** crystallizes in the triclinic $P\overline{1}$ space group (Table S1).

Cages **1**−**3** differ only in their substituents on the periphery, with decreasing size from **2** to **1** to **3**. However, such small variations lead to a dramatic difference in their 3-D crystal packing mode. As shown in Figure 3A, a zigzag linear packing mode has been observed in the crystal structure of cage **1**. This has been driven by the third type of Au^I···Au^I interactions existing between the neighboring cages, with an average Au···Au distance of 3.00 Å. This weak intercage Au^I···Au^I interaction leads to the formation of a single-layer 2-D molecular arrays composing of two kinds of Au(I) chains (Au$_8$ and [Au$_8$]$_\infty$) with continuous Au^I···Au^I interaction along the *a* axis. No polymeric 2-D molecular array has been observed in the crystal structure of cage **2** where a slightly larger phenylethyl substituent has been used, which is in contrast to that of the phenylmethyl substituent in cage **1** (Figure 3B). The anticipated steric effect hinders the formation of the 2-D sheet-like molecular array via
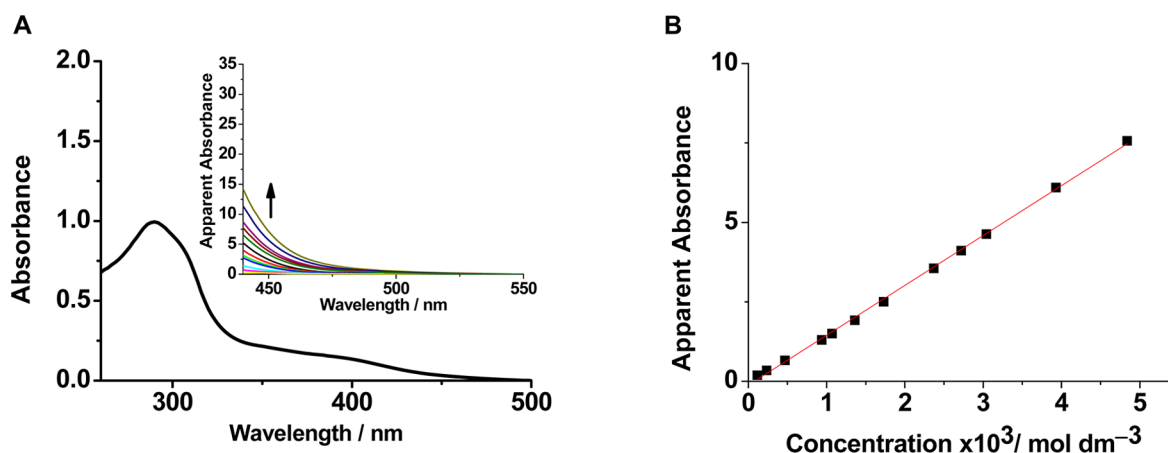
Figure 5. (A) UV−Vis absorption spectrum of complex **2** in dichloromethane. Inset: UV−Vis absorption spectral changes of **2** in dichloromethane as the concentration increases from 1.17×10^{-4} to 4.84×10^{-3} M. The apparent absorbance values have been corrected to a 1 cm path-length equivalence. (B) A plot of absorbance at 450 nm as a function of concentration for complex **2**. Experimental (■) and theoretical (red line) fit to Beer's law.

intermolecular $Au^I \cdots Au^I$ bonding interactions. Interestingly, a continuous $Au^I \cdots Au^I$ interaction-directed two-dimensional molecular array composing of two infinite chains of $[Au_8]_\infty$ without any breakage has been observed in the crystal packing of cage **3** (Figure 3C), where a 2-thienylmethyl substituent is used in the ligand. These layers are loosely packed along the *a* axis. In this case, average intracage $Au^I \cdots Au^I$ distances of 2.85 Å with longer intercage $Au^I \cdots Au^I$ distances of 3.21 Å are observed. The remarkable packing differences in the complexes offer a useful empirical rule for the design of supramolecular gold(I)-containing solid-state materials.

Photophysical and Self-Assembly Studies. The electronic absorption spectra of **1**−**3** (Figures 4A, 5A, and S45) in dichloromethane at 298 K are dominated by high-energy absorption bands at 294 nm (ε_{max} = 178,810 M^{-1} cm^{-1}), 290 nm (ε_{max} = 184,230 M^{-1} cm^{-1}), and 300 nm (ε_{max} = 174,560 M^{-1} cm^{-1}), respectively, which are assigned as metal-perturbed intraligand transitions of the thiocarbamate ligand with reference to the previous studies on Au(I) thiolate complexes.[9] There are additional low-energy shoulders at around 400 nm and low-energy tails at around 450 nm that become more apparent with increasing concentration. The low-energy shoulders and tails are assigned as ligand-to-metal−metal charge transfer LMMCT (thiocarbamate-to-gold−gold) transitions.[9,11]

The intermolecular aggregation process driven by $Au^I \cdots Au^I$ interactions has been further investigated by concentration-dependent studies of complexes **1** and **3** in dichloromethane at room temperature. Upon increasing the concentration of complexes **1** and **3**, the low-energy tail was found to grow in at around 450 nm (Figures 4A and S45A inset). A plot of absorbance at 450 nm with the concentration was found to not follow Beer's law but showed a nonlinear relationship (Figures 4B and S45B), suggesting the self-assembly of the Au_8 cage to give higher oligomers. The presence of higher oligomers is consistent with the proposed 2-D molecular sheet-like networks, as revealed by X-ray diffraction structural analysis. From the straight line plot of $[\mathbf{1}]/(A_{450})^{1/2}$ or $[\mathbf{3}]/(A_{450})^{1/2}$ versus $(A_{450})^{1/2}$ (Figures S46 and S47), a dimerization process involving a monomer−dimer equilibrium has been established, with ε_{max} ($\mathbf{1_2}$) and K determined to be 5945 M^{-1} cm^{-1} and 22,825 M^{-1} for **1**, and ε_{max} ($\mathbf{3_2}$) and K determined to be 6725

M^{-1} cm^{-1} and 5220 M^{-1} for **3**, respectively. In contrast, as a single cage, for the concentration-dependent studies on the single-cage complex **2** up to a concentration of 4.84×10^{-3} M, the growth of absorbance in the low-energy tail was not comparable to those found in complexes **1** and **3** under the same concentration. Instead, a linear plot of absorbance at 450 nm with concentration was obtained, where the Beer's Law has been obeyed (Figures 5A and 5B), suggesting the absence of an intermolecular aggregation process. Interestingly, the plots of absorbances at the shoulder at ca. 400 nm for complexes **1**−**3** all showed an almost linear plot (Figure S48), with much less obvious deviation from the Beer's law for complexes **1** and **3**. It is likely that the shoulder at ca. 400 nm is associated with an assignment of an intramolecular LMMCT transition occurring within the single cage, while the absorption tail at ca. 450 nm is assigned as LMMCT transition associated with extended $Au^I \cdots Au^I$ interactions arising from additional intermolecular interactions of the oligomeric cages. Such an observation is also consistent with the different packing mode observed in their crystal structures among complexes **1**−**3**.

Upon photoexcitation, complexes **1**−**3** emit at 559, 561, and 567 nm in deoxygenated dichloromethane solution at 298 K, respectively, while in the glass state at 77 K, the emission maxima show an obvious blue shift from 559 to 537 nm, from 561 to 518 nm, and from 567 to 531 nm, respectively. The photophysical data of complexes **1**−**3** are summarized in Table S5. With reference to the previous reports on the luminescence studies of Au(I) thiolate complexes,[9,11] the emission bands are tentatively assigned to be derived from triplet excited states of metal-centered (ds/dp) and ligand-to-metal charge transfer character that has been modified by $Au^I \cdots Au^I$ interactions although a mixing of a dithiocarbamate ligand-centered character cannot be completely excluded. Blue shifts in the glass state have also been reported in other related gold(I) sulfido clusters.[10a−c] The smaller Stokes shift at 77 K is probably a result of the increase in rigidity at low temperature, leading to a smaller geometrical distortion in the excited state. The solid state emission spectra at 77 K show obvious differences among complexes **1**−**3**. Complex **2** shows emission at 544 nm while complexes **1** and **3** emit at 624 and 644 nm, respectively (Figure 6). The emission origin of complex **2** is assigned to excited states of triplet LMMCT character derived
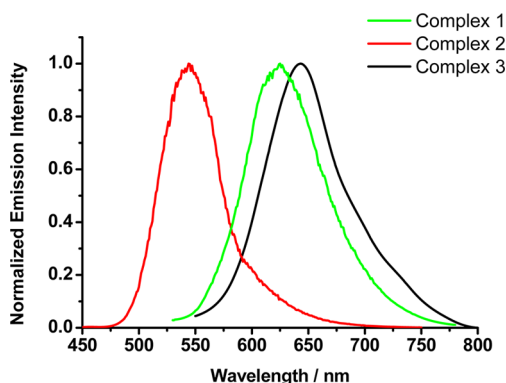
Figure 6. Normalized emission spectra of complexes **1**–**3** in the solid state at 77 K.

from intramolecular $Au^I \cdots Au^I$ interactions. An additional excitation band beyond 450 nm has been observed in the excitation spectra of **1** and **3**, which is not found in complex **2** (Figure S49). The excitation band beyond 450 nm, which coincides with the absorption shoulder formed at about 450 nm in the UV–vis spectra with increasing concentration of complexes **1** and **3**, suggests that the 624 and 644 nm emission are derived from the supramolecular 2-D molecular sheet-like networks with intermolecular $Au^I \cdots Au^I$ interactions, and the origin is assigned to excited states of triplet LMMCT (thiocarbamate-to-gold–gold) character derived from an extension of the $Au^I \cdots Au^I$ interactions via additional inter-molecular supramolecular assembly processes.

Luminescence Switching and Sensing for Silver(I) Ions. The development of chemosensors for the selective binding of various biological and environmental relevant cations has gained considerable attention in recent years.[20] Luminescence sensing of cations, such as Hg^{2+}, Pb^{2+}, Ag^+, and Cu^{2+} is particularly challenging because these transition-metal ions commonly act as quenchers via the electron transfer and intersystem crossing (ISC) processes. In this work, attempts have been made to explore the use of the 3-D neutral cage-like supramolecular complexes with deep cavitand and dithiocarba-mate-bridged extended $Au^I \cdots Au^I$ interactions for the study of their highly selective proof-of-concept chemosensing for various transition-metal ions such as Zn^{2+}, Hg^{2+}, Cd^{2+}, Ni^{2+}, Pb^{2+}, Co^{2+}, Mn^{2+}, Fe^{3+}, Cu^{2+}, and Ag^+ (Figures S50–S55).

Among the transition-metal ions studied, the neutral electron-rich $\{Au_8L_2\}$ supramolecular cages have been demonstrated to show promising performance for the selective luminescence sensing of Ag^+ in the presence of the aforementioned competitive ions. Cages **1**–**3** were found to emit at 559, 561, and 567 nm, respectively, when excited at 430 nm in dichloromethane as free receptors. Upon addition of one equivalent of silver(I) ion into cages **1**–**3** in $CHCl_3$–CH_3CN (20:1 v/v), significant red shifts of the emission from 559 to 660 nm (cage **1**), 561 to 663 nm (cage **2**), and 567 to 630 nm (cage **3**) were observed upon excitation at 430 nm, with a red shift of 65–100 nm (1763–2743 cm^{-1}) (Figures 7B,C and S53). The luminescence intensity of **2** in the presence of 2 equiv $AgPF_6$ has been increased by about 35-fold as compared to that of the silver(I)-free cage **2**. There are no further changes in the luminescence of cages **1**–**3** even in the presence of an excess amount of $AgPF_6$ (molar ratio of $[AgPF_6]/[cage 1]$ or $[AgPF_6]/[cage 2]$ reached 4:1). The observed broad emission bands centered at 660 nm, 663 and 630 nm are assigned to arise from the strong interaction between the Ag^+ and gold(I)-containing cages in solution and are attributed to the extension of the $Au^I \cdots Au^I$ interaction via the formation of $Au^I \cdots Ag^I$ metallophilic interactions, giving rise to $Au^I \cdots Au^I \cdots Ag^I$ ^{3}LMMCT emission (Figure 7). Interestingly, removal of Ag^+ with the use of an excess of tetraethylammonium iodide (TEAI in $CHCl_3$–CH_3CN (20:1 v/v) has led to the disappearance of the red emission and the recovery of green luminescence and the precipitation of AgI, indicating the reversibility of the luminescence sensing process, which can be repeated for at least four times with insignificant decay.

In order to provide further insights into the luminescence sensing of silver ions, the interactions of the $\{Au_8L_2\}$ supramolecular cages with Ag^I ions have been explored by ^1H NMR studies. The ^1H NMR spectral changes of complex **2** upon addition of $AgPF_6$ (0–8 equiv) are shown in Figures S57 and S58. In contrast to the ^1H NMR spectrum of free cage **2**, three doublet signals were observed at δ 6.71, 6.26, and 5.87 ppm which became less complicated and were upfield-shifted by about 0.3 ppm upon addition of 1 equiv of $AgPF_6$. The other protons on the $-CH_3$ and $-CH_2$ groups of the receptor cage **2** were also found to be affected and become broad signals (Figures S60 and S61). These results indicated that the distorted dimeric cage would be changed to a more symmetrical structure upon interaction with silver ions through $Au^I \cdots Ag^I$
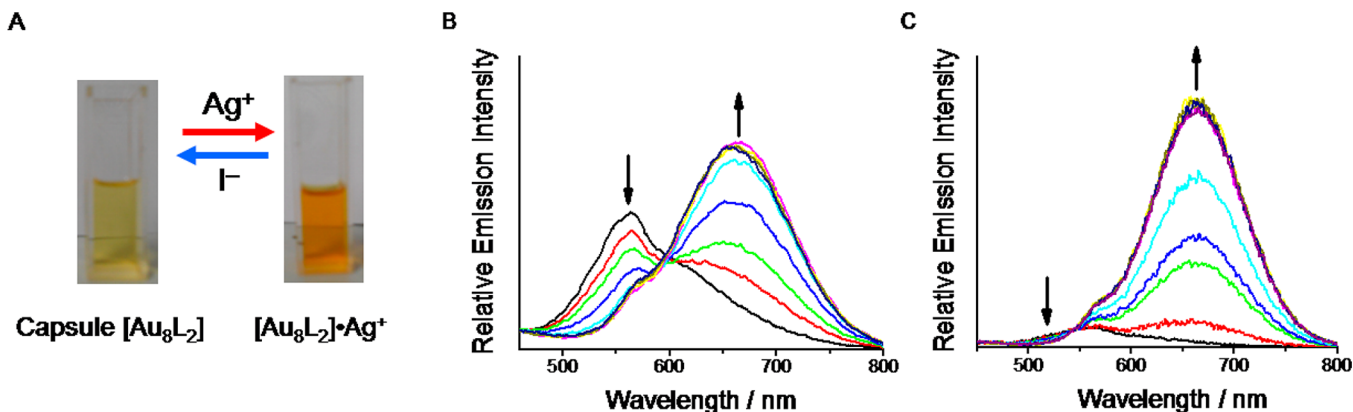

Figure 7. Photograph of cages **1** and **2** as photoswitching sensors from free cage to cage with silver ions recycled using tetraethylammonium iodide in $CHCl_3$ (A). Emission spectral changes of (B) cage **1** $\{Au_8L_2\}_n$ and (C) cage **2** titrated with $AgPF_6$ (from 0–2 equiv) in $CHCl_3$–CH_3CN (20:1 v/v) solution with 1 mM $^nBu_4N(PF_6)$ as supporting electrolyte (λ_{ex} = 430 nm).

metallophilic and $Ag^I{\cdots}\pi$ interactions in the supramolecular cage **2** and is consistent with the luminescence changes associated with the formation of these $Au^I{\cdots}Au^I{\cdots}Ag^I$ and $Ag^I{\cdots}\pi$ interactions.

As shown in Figure S56, similar results have been obtained for cage **1** with silver ions. The signals observed ranging from δ 5.94 ppm to 7.53 ppm, which were ascribed to the protons of the phenyl groups on the ligands, became less complicated and showed remarkable upfield shift in the ^1H NMR spectrum of cage **1** upon addition of 1 equiv of Ag^+ ions. At the same time, all the signals gradually became broad with the increasing excess of silver ions in the solution media. This has further supported the formation of a $1{\cdot}Ag^+$ adduct. In addition, cage **3** displays a high selectivity toward silver ions in solution media, and similar observations have been found in its ^1H NMR spectrum (Figure S59) and emission spectrum. Unfortunately, efforts to crystallize the host−guest complexes were in vain, rendering the detailed mechanistic studies difficult.

In summary, we have successfully designed and synthesized a class of multidimensional gold(I) supramolecular oligomers. The $Au^I{\cdots}Au^I$ bonding interactions have provided the driving force to induce the self-assembly of a unique gold(I)-containing supramolecular network, constructed from 3-D cavitand-based coordination cages. ^1H NMR, MALDI-TOF-MS and synchrotron radiation single-crystal X-ray diffraction analysis have been used to characterize the target complexes **1−3**. The conformational flexibility of the calix[4]arene-based organic bridging ligands in the cone conformation and $Au^I{\cdots}Au^I$ bonding interactions have played an important role in the controlled construction of sheet-like molecular arrays and dumbbell-shaped supramolecular cages. These interesting results would open up new possibilities and opportunities for the self-assembly of a diverse array of 3-D and 2-D molecular cages and supramolecular wires from simple metal−metal bonding subunits. Gold(I) complexes **1−3** have been shown to exhibit green phosphorescence, which could be exploited as potential highly selective phosphorescent sensor materials for silver ions via heterometallic Au···Ag bonding interactions. Based on the flexible cage-like calix[4]arene dimers, extension of the work toward molecular recognition and catalytic reactivity studies is in progress.

■ EXPERIMENTAL SECTION

Materials and Reagents. Unless otherwise stated, all manipulations were carried out under nitrogen using standard Schlenk techniques. Solvents were dried by conventional methods and were freshly distilled under nitrogen before use. The starting materials 5,11,17,23-tetraformyl-25,26,27,28-tetrapropoxycalix[4]arene[18] and [Au(tht)Cl] (tht = tetrahydrothiophene)[11] were prepared according to reported methods. All other chemicals were purchased from commercial sources and used as received. Tetra-n-butylammonium hexafluorophosphate was recrystallized twice from absolute ethanol before use.

Physical Measurements and Instrumentation. ^1H and ^{13}C NMR spectra were recorded on Bruker Avance 400 spectrometer at 298 K. The MALDI-TOF mass spectra were collected on a Bruker Biflex instrument. The high-resolution ESI-MS spectra were collected on a Bruker FT-ICR-MS APEX III7.0 instrument. The high-resolution CSI-TOF-MS spectra were collected on a JMS-T100CS instrument. The UV−vis spectra were obtained using a Hewlett-Packard 8452A diode array spectrophotometer. Steady-state excitation and emission spectra were recorded on a Spex Fluorolog-3 model FL3-211 fluorescence spectrofluorometer equipped with an R2658P PMT detector. All solutions for photophysical studies were prepared under a high vacuum in a 10 cm^3 round-bottomed flask equipped with a side

arm 1 cm fluorescence cuvette and sealed from the atmosphere by a Rotaflo HP6/6 quick-release Teflon stopper. Solutions were rigorously degassed on a high-vacuum line in a two-compartment cell with no less than four successive freeze−pump−thaw cycles. Photophysical measurements in low-temperature glass were carried out with the sample solution loaded in a quartz tube inside a quartz-walled Dewar flask. Liquid nitrogen was placed into the Dewar flask for low-temperature (77 K) photophysical measurements. Excited-state lifetimes of solution samples were measured using a conventional laser system. The excitation source used was the 355 nm output (third harmonic, 8 ns) of a Spectra-Physics Quanta-Ray Q-switched GCR-150 pulsed Nd:YAG laser (10 Hz). Luminescence decay signals were detected by a Hamamatsu R928 photomutiplier tube, recorded on a Tektronix model TDS-620A (500 MHz, 2GS/s) digital oscilloscope, and analyzed using a program for exponential fits on a personal computer.

The general synthesis of tetrakis(dithiocarbamato)-25,26,27,28-tetrapropoxycalix[4]arene ligands K_4L^n (n = 1−3). KOH (1 mmol) and CS_2 (1 mmol) were added to a solution of the respective tetra-aminocalix[4]arene (0.25 mmol) in CH_3OH (2 mL). The mixture was stirred at room temperature for 4 h, after which a yellow precipitate started to form. The yellow solid was filtered off, washed with diethyl ether (10 mL), and dried under vacuum. The light-yellow products were used for further experiments after washing with water.

K_4L^1: yellow solid (Yield: 350 mg, 75%). mp 210−215 °C. ^1H NMR (400 MHz, DMSO-d_6, 298 K): δ = 7.29−7.06 (m, 20H, C_6H_5- CH_2N), 6.62 (s, 8H, $C_6H_2-CH_2-C_6H_2$), 5.16 (s, 8H, Ar−CH_2−N), 4.84 (s, 8H, Ar−CH_2−N), 4.32 (d, J = 12.6 Hz, 4H, $C_6H_2-CH_2-$ C_6H_2), 3.76 (t, J = 7.4 Hz, 8H, $OCH_2CH_2CH_3$), 3.03 (d, J = 12.6 Hz, 4H, $C_6H_2-CH_2-C_6H_2$), 1.92 (ψ-sext, 8H, $OCH_2CH_2CH_3$), 1.08− 0.98 (t, J = 7.4 Hz, 12H, $OCH_2CH_2CH_3$). ^{13}C NMR (100 MHz, DMSO-d_6, 25 °C, ppm): δ 214.93, 156.06, 137.70, 135.00, 128.95, 128.66, 128.13, 126.29, 76.90, 55.25, 33.01, 23.27, 18.92, 10.68. IR (KBr, ν/cm^{-1}): 1128 (C−N), 1028 (C═S), 1614 (Ar−H), 771 (C−H). MALDI-TOF-MS (CH_3OH) m/z: $[M - CS_2 - 4K^+ + 5H^+]^+$, calcd for $C_{75}H_{87}N_4O_5S_6^+$; 1316.9, found, 1316.4; $[M - 2CS_2 - 4K^+ + 2H_2O + 5H^+]^+$, calcd for $C_{74}H_{89}N_4O_6S_4^+$; 1257.57, found, 1257.5.

K_4L^2: light-yellow solid (Yield: 345 mg, 78%). mp 220−223 °C. ^1H NMR (400 MHz, DMSO-d_6, 298 K): δ = 7.11−7.23 (20H, Ar−Ar), 6.73 (s, 8H, Ar−CH_2), 4.35 (4H, J = 12.8 Hz, Ar−CH_2−Ar), 3.92 (t, J = 7.4 Hz, 16H, Ar−CH_2−N−CH_2), 3.76 (8H, Ar−CH_2−O), 3.06 (t, J = 12.8 Hz, 4H, Ar−CH_2−Ar), 2.88 (t, 8H, J = 12.4 Hz, Ar−CH_2− CH_2−N), 1.92 (ψ-sext, 8H, CH_2OCH_2), 1.08−0.98 (t, J = 7.4 Hz, 12H, $CH_3CH_2CH_2O$). ^{13}C NMR (100 MHz, DMSO-d_6, 25 °C, ppm): δ 206.53, 156.21, 142.37, 138.12, 137.74, 134.06, 128.35, 127.45, 78.11, 56.57, 37.43, 31.11, 23.27, 18.94, 11.35, 10.54. IR (KBr, ν/ cm^{-1}): 1247 (C−N), 1128 (C═S), 1633 (Ar−H), 789 (C−H). MALDI-TOF-MS (CH_3OH) m/z: $[M - 4K^+ + 2DMSO + Na + 4H^+]^+$, calcd for $C_{82}H_{98}N_4NaO_5S_9^+$; 1529.49, found, 1528.6; $[M - 2K^+ + 2DMSO + 3H^+]^+$, calcd for $C_{84}H_{103}K_2N_4O_6S_{10}^+$; 1661.44; found, 1659.7; $[M - K^+ + 3DMSO + 2H^+]^+$, calcd for $C_{86}H_{110}K_3N_4O_8S_{11}^+$; 1795.42; found, 1796.6.

K_4L^3: yellow solid (Yield: 315 mg, 65%). mp 210−215 °C. ^1H NMR (400 MHz, DMSO-d_6, 298 K): δ = 7.11−7.23 (20H, Ar−Ar), 6.73 (s, 8H, Ar−CH_2), 4.35 (4H, J = 12.6 Hz, Ar−CH_2−Ar), 3.92 (t, J = 7.4 Hz, 16H, Ar−CH_2−N−CH_2), 3.76 (8H, J = 7.4 Hz, Ar−CH_2− O), 3.06 (t, J = 12.6 Hz, 4H, Ar−CH_2−Ar), 2.88 (d, 8H, J = 12.4 Hz, Ar−CH_2−CH_2−N), 1.92 (ψ-sext, 8H, CH_2OCH_2), 0.98 (12H, J = 7.4 Hz, $CH_3CH_2CH_2O$). ^{13}C NMR (100 MHz, DMSO-d_6, 25 °C, ppm): δ 207.38, 158.73, 141.57, 134.29, 133.26, 128.30, 127.45, 126.15, 78.63, 56.52, 37.16, 23.25, 18.94, 14.92, 10.69. IR (KBr, ν/cm^{-1}): 1249 (C−N), 1137 (C═S), 1661 (Ar−H), 791 (C−H). MALDI-TOF-MS (CH_3OH) m/z: $[M - CS_2 - 3K^+ + 4H^+]^+$, calcd for $C_{67}H_{76}KN_4O_4S_{10}^+$; 1359.27, found, 1359.2; $[M - 2CS_2 - 3K^+ + 4H^+]^+$, calcd for $C_{66}H_{76}KN_4O_4S_8^+$, 1283.33; found, 1281.3; $[M - 3CS_2 - 4K^+ + 2Na^+ + CH_3OH + 3H^+]^+$, calcd for $C_{66}H_{79}N_4Na_2O_5S_6^+$, 1245.42; found, 1245.3.

The General Preparation Procedure of Gold(I) Complexes 1−3. A solution of [Au(tht)Cl] (0.100 mmol) in dichloromethane (3 mL) was added to the mixture of tetrakis(dithiocarbamato)calix[4]-

arene K_4L (0.025 mmol) in methanol (3 mL). The reaction was stirred for 24 h until precipitation of the orange-red product was complete, and the solvent was removed under vacuum. The crude product was dissolved in dichloromethane (3 mL) and purified by flash chromatography with hexane-CH_2Cl_2 (1:7, v/v) to give the target gold(I) complex as a yellow solid. The solid was dissolved in 5 mL CH_3OH–$CHCl_3$ (1:4, v/v), and slow diffusion of diethyl ether into the mixture at −5 °C led to the formation of block red crystals that are suitable for X-ray diffraction analysis.

Complex 1. Single crystals of complex **1** were obtained by slow diffusion of diethyl ether into the solution at low temperature (−5 °C) to give complex **1** as diffraction-quality red block crystals. Yield: 65%. ^{1}H NMR (400 MHz, $CDCl_3$, 298 K): δ = 7.51 (d, 8H, J = 4.0 Hz, Ar—C—N), 7.01 (s, 2H, Ar(Calix)), 6.93 (t, 8H, J = 7.5 Hz, Ar—C—N), 6.81 (s, 2H, Ar(Calix)), 6.69 (d, 4H, J = 6.9 Hz, Ar—C—N), 6.44 (s, 2H, Ar(Calix)), 6.34 (d, 2H, J = 15.0 Hz, Ar—CH_2—N—CH_2—Calix), 6.24 (d, 2H, J = 13.6 Hz, Ar—CH_2—N—CH_2—Calix), 6.12 (d, 3H, J = 16.1 Hz, Ar—CH_2—N—CH_2-Calix), 5.98 (s, 2H, Ar(Calix)), 5.55 (d, 2H, J = 16.4 Hz, Ar—CH_2—N—CH_2-Calix), 4.90 (d, 2H, J = 16.1 Hz, Ar—CH_2—N—CH_2-Calix), 4.73 (m, 4H, Ar—CH_2—N-Calix), 4.30 (m, 2H, Ar—CH_2—N—CH_2-Calix), 4.28–4.21 (m, 4H, Ar—CH_2—Ar), 3.97 (m, 2H, J = 8.1 Hz, Ar—O—CH_2), 3.86 (m, 2H, J = 8.2 Hz, Ar—O—CH_2), 3.41 (t, 4H, J = 6.7 Hz, Ar—O—CH_2), 3.02 (d, 2H, J = 13.3 Hz, Ar—CH_2—Ar), 2.87 (d, 2H, J = 13.3 Hz, Ar—CH_2—Ar), 1.97 and 1.75 (ψ-sext, 8H, $CH_2CH_2CH_3O$), 1.23 and 1.09 (t, 12H, J = 7.4 Hz, $CH_3CH_2CH_2O$). ^{13}C NMR (100 MHz, DMSO-d_6, 25 °C, ppm): δ 213.72, 209.13, 157.03, 156.23, 138.92, 138.11, 136.65, 130.29, 129.45, 126.83, 71.62, 70.82, 70.62, 62.38, 47.97, 33.41, 29.69, 23.44, 23.09, 22.69, 14.10, 13.6, 10.81, 9.94. IR (KBr, ν/cm^{-1}): 1661 (Ar—H), 1247 (C—N), 1147 (C=S). MALDI-TOF-MS (CHCl$_3$, m/z): [Au$_8$L$^1_2$ + H$^+$]$^+$, calcd for $C_{152}H_{161}Au_8N_8O_8S_{16}$$^+$; 4312.5, found, 4312.0; [Au$_7$L$^1_2$ + 2H$^+$]$^+$, calcd for $C_{152}H_{162}Au_7N_8O_8S_{16}$$^+$; 4116.55, found, 4115.55; [Au$_6$L$^1_2$ + 3H$^+$]$^+$, calcd for $C_{152}H_{163}Au_6N_8O_8S_{16}$$^+$; 3919.59, found, 3914.5. Elemental analyses calcd (%) for $C_{152}H_{160}Au_7N_8O_8S_{16}$·4CH$_2Cl_2$: C, 41.31; H, 3.89; N, 2.35. Found: C, 41.07; H, 3.92; N, 2.32.

Complex 2. Single crystals of complex **2** were obtained by slowly evaporating the solvents from a CH_3OH–$CHCl_3$ (1:4, v/v) solution of the complex at room temperature. Yield: 75%. ^{1}H NMR (400 MHz, $CDCl_3$, 298 K): δ = 7.46, 7.41, 7.32, 7.17, 7.10, and 6.94 (t, 20H, J = 7.2 Hz, Ar—C—N), 7.07, 6.76, 6.50, and 6.24 (s, 8H, Ar(Calix)), 6.06 and 5.51 (d, 4H, J = 13.7 Hz, Ar—CH_2CH_2—N), 4.98, 4.72, 3.42, and 3.25 (t, 8H, J = 8.6 Hz, ArCH_2CH_2N—CH_2-Calix), 4.45 and 4.38 (d, 4H, J = 13.1 Hz, Ar—CH_2—Ar), 4.57 and 4.17 (4H, J = 13.7 Hz, Ar—CH_2CH_2—N), 4.08, 3.92, and 3.61 (d, 8H, J = 7.2 Hz, Ar—O—CH_2), 3.83, 3.29, and 3.18 (m, 8H, ArCH_2CH_2—N), 3.18 and 3.08 (4H, Ar—CH_2—Ar), 2.0 and 1.84 (ψ-sext, 8H, $CH_3CH_2CH_2O$), 1.09 and 0.92 (t, 12H, J = 7.3 Hz, $CH_3CH_2CH_2O$). ^{13}C NMR (100 MHz, DMSO-d_6, 25 °C, ppm): δ 213.09, 149.07, 148.92, 137.78, 133.45, 129.05, 127.64, 70.92, 42.33, 32.11, 29.88, 23.75, 22.88, 14.31, 14.06, 13.97, 11.83, 10.10. IR (KBr, ν/cm^{-1}): 1642 (Ar—H), 1219 (C—N), 1138 (C=S). MALDI-TOF-MS (CHCl$_3$, m/z): [Au$_8$L$^2_2$ + H$^+$]$^+$, calcd for $C_{160}H_{177}Au_8N_8O_8S_{16}$$^+$; 4425.5, found, 4425.5; [Au$_7$L$^2_2$ + H$_2$O + H$^+$]$^+$, calcd for $C_{160}H_{180}Au_7N_8O_9S_{16}$$^+$; 4247.5, found, 4241.55. Elemental analyses calcd (%) for $C_{160}H_{176}Au_8N_8O_8S_{16}$: C, 43.45; H, 4.08; N, 2.51. Found: C, 43.47; H, 4.11; N, 2.48.

Complex 3. Single crystals of complex **3** were obtained by slow diffusion of diethyl ether into the solution at low temperature (−5 °C) to give complex **3** as diffraction-quality red block crystals. Yield: 75%. ^{1}H NMR (400 MHz, $CDCl_3$, 298 K): δ = 7.37, (m, 2H, thienyl-H) 7.25, (d, 4H, J = 3.2 Hz, thienyl-H), 7.06 (d, 2H, J = 3.5 Hz, thienyl-H), 6.92 (d, 2H, J = 5.0 Hz, thienyl-H), 6.58 (m, 2H, thienyl-H), 6.99, 6.76, 6.37, and 6.25 (s, 8H, Ar(Calix)), 6.23 (m, 2H, thienyl—CH_2—N), 6.15 (d, J = 8.7 Hz, 2H, thienyl—CH_2—N), 6.05 (d, 2H, J = 8.7 Hz, thienyl—CH_2—N—CH_2—Calix), 5.49 (d, 2H, J = 16.3 Hz, thienyl—CH_2—N—CH_2—Calix), 4.96 (d, 2H, J = 8.1 Hz, thienyl—CH_2—N), 4.92 (d, 2H, J = 8.4 Hz, thienyl—CH_2—N—CH_2—Calix), 4.86 (d, 2H, J = 16.3 Hz, thienyl—CH_2—N—CH_2—Calix), 4.37, 4.30, 3.08, and 2.97 (d, 8H, J = 13.1 Hz, Ar—CH_2—Ar), 4.22 (d, 2H, J = 14.0 Hz, thienyl—CH_2—N), 4.08, 3.92, and 3.60 (d, 8H, J = 8.5 Hz, Ar—O—CH_2), 1.98

and 1.86 (ψ-sext, 8H, $CH_3CH_2CH_2O$), 1.13 and 0.93 (t, 12H, J = 7.4 Hz, $CH_3CH_2CH_2O$). ^{13}C NMR (100 MHz, DMSO-d_6, 25 °C, ppm): δ 213.07, 209.95, 205.44, 157.23, 155.27, 137.85, 136.95, 136.36, 133.49, 129.22, 127.06, 126.69, 125.60, 77.65, 77.22, 76.8, 71.04, 70.83, 48.20, 42.22, 31.11, 29.87, 23.61, 23.56, 13.97, 11.06, 10.07. IR (KBr, ν/cm^{-1}): 1649 (Ar—H), 1210 (C—N), 1121 (C=S). MALDI-TOF-MS (CHCl$_3$, m/z): [Au$_8$L$^3_2$ + H$^+$]$^+$, calcd for $C_{136}H_{145}Au_8N_8O_8S_{24}$$^+$; 4361.17, found, 4361.0; [Au$_7$L$^3_2$ + 2H$^+$]$^+$, calcd for $C_{136}H_{146}Au_7N_8O_8S_{24}$$^+$; 4165.21, found, 4164.0; [Au$_6$L$^3_2$ + 3H$^+$]$^+$, calcd for $C_{136}H_{147}Au_6N_8O_8S_{24}$$^+$; 3969.24, found, 3965.0. Elemental analyses calcd (%) for $C_{136}H_{144}Au_8N_8O_8S_{24}$: C, 37.43; H, 3.31; N, 2.63. Found: C, 37.39; H, 3.28; N, 2.64.

■ ASSOCIATED CONTENT

ⓢ Supporting Information

Crystallographic information for complexes 1−3 in CIF format. Details of the procedures for the syntheses of all organic ligands and complex **1−3**. The additional figures as supporting data. This material is available free of charge via the Internet at http://pubs.acs.org.

■ AUTHOR INFORMATION

Corresponding Authors
yusy@ruc.edu.cn
wwyam@hku.hk

Notes
The authors declare no competing financial interest.

■ ACKNOWLEDGMENTS

■ REFERENCES

(1) (a) Schmidbaur, H. *Chem. Soc. Rev.* **1995**, *24*, 391. (b) Schmidbaur, H.; Schier, A. *Chem. Soc. Rev.* **2008**, *37*, 1931. (c) Schmidbaur, H.; Schier, A. *Chem. Soc. Rev.* **2012**, *41*, 370.

(2) Pyykko, P. *Chem. Rev.* **1997**, *97*, 597.

(3) (a) Puddephatt, R. J. *Coord. Chem. Rev.* **2001**, *216*, 313. (b) Puddephatt, R. J. *Chem. Soc. Rev.* **2008**, *37*, 2012. (c) Laguna, A. *Modern Supramolecular Gold Chemistry*; VCH, Weinheim, Germany, 2008.

(4) Hall, K. P.; Mingos, D. M. P. *Prog. Inorg. Chem.* **1984**, *32*, 237.

(5) (a) Leung, K. H.; Phillips, D. L.; Tse, M. C.; Che, C. M.; Miskowski, V. M. *J. Am. Chem. Soc.* **1999**, *121*, 4799. (b) Fu, W.-F.; Chan, K. C.; Miskowski, V. M.; Che, C. M. *Angew. Chem., Int. Ed.* **1999**, *38*, 2783.

(6) (a) Vogler, A.; Kunkely, H. *Chem. Phys. Lett.* **1988**, *150*, 135. (b) Mingos, D. M. P.; Yau, J.; Menzer, S.; Williams, D. J. *Angew. Chem., Int. Ed. Engl.* **1995**, *34*, 1894. (c) McCleskey, T. M.; Gray, H. B. *Inorg. Chem.* **1992**, *31*, 1733.

(7) Fung, E. Y.; Olmstead, M. M.; Vickery, J. C.; Balch, A. L. *Coord. Chem. Rev.* **1998**, *171*, 151.

(8) (a) Yam, V. W.-W.; Cheng, E. C.-C. *Top. Curr. Chem.* **2007**, *281*, 269. (b) Yam, V. W.-W.; Cheng, E. C.-C. *Chem. Soc. Rev.* **2008**, *37*, 1806. (c) Yam, V. W.-W.; Lo, K. K.-W. *Chem. Soc. Rev.* **1999**, *28*, 323.

(9) (a) Jones, W. B.; Yuan, J.; Narayanaswamy, R.; Young, M. A.; Elder, R. C.; Bruce, A. E.; Bruce, M. R. M. *Inorg. Chem.* **1995**, *34*, 1996. (b) Forward, J. M.; Bohmann, D.; Fackler, J. P.; Staples, R. J. *Inorg. Chem.* **1995**, *34*, 6330. (c) Tang, S. S.; Chang, C.-P.; Lin, I. J. B.; Liou, L.-S.; Wang, J.-C. *Inorg. Chem.* **1997**, *36*, 2294. (d) Yam, V. W.-W.; Li, C.-K.; Chan, C.-L. *Angew. Chem., Int. Ed.* **1998**, *37*, 2857. (e) Li, C.-K.; Lu, X.-X.; Wong, M.-C.; Chan, C.-L.; Zhu, N.; Yam, V. W.-W. *Inorg. Chem.* **2004**, *43*, 7421.

(10) (a) Yam, V. W.-W.; Cheng, E. C.-C.; Zhu, N. *Angew. Chem., Int. Ed.* **2001**, *40*, 1763. (b) Yam, V. W.-W.; Cheng, E. C.-C.; Cheung, K. K. *Angew. Chem., Int. Ed.* **1999**, *38*, 197. (c) Yam, V. W.-W.; Cheng, E. C.-C.; Zhou, Z.-Y. *Angew. Chem., Int. Ed.* **2000**, *39*, 1683. (d) Yip, S.-K.; Cheng, E. C.-C.; Yuan, L.-H.; Zhu, N.; Yam, V. W.-W. *Angew. Chem., Int. Ed.* **2004**, *43*, 4954.

(11) (a) Yu, S.-Y.; Zhang, Z.-X.; Cheng, E. C.-C.; Li, Y.-Z.; Yam, V. W.-W.; Huang, H.-P.; Zhang, R. *J. Am. Chem. Soc.* **2005**, *127*, 17994. Highlighted by Szuromi, P. D. *Science* **2005**, *310*, 1745. (b) Yu, S.-Y.; Sun, Q.-F.; Lee, T. K.-M.; Cheng, E. C.-C.; Li, Y.-Z.; Yam, V. W.-W. *Angew. Chem., Int. Ed.* **2008**, *47*, 4551. (c) Sun, Q.-F.; Lee, T. K.-M.; Li, P.-Z.; Yao, L.-Y.; Huang, J.-J.; Huang, J.; Yu, S.-Y.; Li, Y.-Z.; Yam, V. W.-W. *Chem. Commun.* **2008**, *43*, 5514. (d) Lee, T. K.-M.; Zhu, N.-Y.; Yam, V. W.-W. *J. Am. Chem. Soc.* **2010**, *132*, 17646.

(12) (a) Jia, G.; Payne, N. C.; Vittal, J. J.; Puddephatt, R. J. *Organometallics* **1993**, *12*, 4771. (b) Irwin, M. J.; Jia, G.; Payne, N. C.; Puddephatt, R. J. *Organometallics* **1996**, *15*, 51.

(13) (a) Kishmura, A.; Yamshita, T.; Aida, T. *J. Am. Chem. Soc.* **2005**, *127*, 179. (b) Burini, A.; Fackler, J. P., Jr.; Galassi, R.; Grant, T. A.; Omary, M. A.; Rawashdeh-Omary, M. A.; Pietroni, B. R.; Staples, R. J. *J. Am. Chem. Soc.* **2000**, *122*, 11264. (c) Vickery, J. C.; Olmstead, M. M.; Fung, E. Y.; Balch, A. L. *Angew. Chem., Int. Ed. Engl.* **1997**, *36*, 1179. (d) Akerström, S. *Ark. Kemi* **1959**, *14*, 387. (e) Calabro, D. C.; Harrison, B. A.; Palmer, G. T.; Moguel, M. K.; Rebbert, R. L.; Burmeister, J. L. *Inorg. Chem.* **1981**, *20*, 4311. (f) Bardaji, M.; Laguna, A.; Laguna, M. *J. Chem. Soc., Dalton Trans.* **1995**, 1255. (g) van Zyl, W. E.; López-de-Luzuriaga, J. M.; Fackler, J. P., Jr. *J. Mol. Struct.* **2000**, *516*, 99. (h) van Zyl, W. E.; López-de-Luzuriaga, J. M.; Mohamed, A. A.; Staples, R. J.; Fackler, J. P., Jr. *Inorg. Chem.* **2002**, *41*, 4579.

(14) (a) Lee, Y. A.; McGarrah, J. E.; Lachicotte, R. J.; Eisenberg, R. *J. Am. Chem. Soc.* **2002**, *124*, 10662. (b) Mansour, M. A.; Connick, W. B.; Lachicotte, R. J.; Gysling, H. J.; Eisenberg, R. *J. Am. Chem. Soc.* **1998**, *120*, 1329.

(15) (a) McArdle, C. P.; Jennings, M. C.; Vittal, J. J.; Puddephatt, R. J. *Chem.—Eur. J.* **2001**, *7*, 3572. (b) McArdle, C. P.; Van, S.; Jennings, M. C.; Puddephatt, R. J. *J. Am. Chem. Soc.* **2002**, *124*, 3959. (c) de Silva, N.; Ha, J.-M.; Solovyov, A.; Nigra, M. M.; Ogino, I.; Yeh, S. W.; Durkin, K. A.; Katz, A. *Nat. Chem.* **2010**, *2*, 1062.

(16) (a) Sauvage, J. P. *Acc. Chem. Res.* **1998**, *31*, 611. (b) Lehn, J.-M. *Angew. Chem.* **1988**, *100*, 91. (c) Fujita, M.; Tominaga, M.; Hori, A.; Therrien, B. *Acc. Chem. Res.* **2005**, *38*, 369. (d) Stang, P. J.; Leininger, S.; Olenyuk, B. *Chem. Rev.* **2000**, *100*, 853. (e) Jin, P.; Dalgarno, S. J.; Barnes, C.; Teat, S. J.; Atwood, J. L. *J. Am. Chem. Soc.* **2008**, *130*, 17262.

(17) (a) Cotton, F. A.; Murillo, C. A.; Walton, R. A. *Multiple Bonds between Metal Atoms*; Springer: New York, 2005. (b) Roth, S. *One-dimensional Metals*; VCH: Weinheim, 1995. (c) Ferraro, J. R.; Williams, J. M. *Introduction to Synthetic Electrical Conductors*; Academic Press: Waltham, MA, 1987. (d) Miller, J. S. *Extended Linear Chain Compounds*; Plenum: Frankfurt, Germany, 1982. (e) Rau, H. In *Photochromism Molecules and Systems*; Dürr, H., Bouas-Laurent , H., Eds.; Elsevier: Amsterdam, 1990; Chpt. 4. (f) Balzani, V.; Scandola, F. *Supramolecular Photochemistry*; Horwood: Chichester, 1991; Chpt. 7. (g) Balzani, V.; Credi, A.; Venturi, M. Molecular Devices and Machines. *Concepts and Perspectives for the Nanoworld*, 2nd ed.; Wiley: Hoboken, NJ, 2008.

(18) (a) Cram, D. J.; Cram, M. J. *Container Molecules and Their Guests, Monographs in Supramolecular Chemistry*; Stoddart, J. F., Ed.; The Royal Society of Chemistry, Cambridge, 1994. (b) Gutsche, C. D. *Calixarenes*; Stoddart, J. F., Ed.; The Royal Society of Chemistry: Cambridge, 1989. (c) *Calixarenes in the Nanoworld*; Vicens, J., Harrowfield, J., Baklouti, L., Eds.; Springer: New York, 2007. (d) Arduini, A.; Fabbi, M.; Mantovani, M.; Mirone, L.; Pochini, A.; Secchi, A.; Ungaro, R. *J. Org. Chem.* **1995**, *60*, 1454. (e) Botana, E.; Silva, E. Da; Benet-Buchholz, J.; Ballester, P.; de Mendoza, J. *Angew. Chem., Int. Ed.* **2007**, *46*, 198. (f) Castellano, R. K.; Rudkevich, D. M.; Rebek, J., Jr. *J. Am. Chem. Soc.* **1996**, *118*, 10002.

(19) CCDC 938806 (complex **1**), 938807 (complex **2**) and 968915 (complex **3**) contain the supplementary crystallographic data for this paper. These data can be obtained free of charge from The Cambridge Crystallographic Data Centre via www.ccdc.cam.ac.uk/data_request/cif.

(20) (a) Czarnik, A. W. In *Fluorescent Chemosensors for Ion and Molecule Recognition*; American Chemical Society, Washington, DC, 1993. (b) de Silva, A. P.; Gunaratne, H. Q. N.; Gunnlaugsson, T.; Huxley, A. J. M.; McCoy, C. P.; Rademacher, J. T.; Rice, T. E. *Chem. Rev.* **1997**, *97*, 1515. (c) Nolan, E. M.; Lippard, S. J. *Chem. Rev.* **2008**, *108*, 3443. (d) Cho, D. G.; Sessler, J. L. *Chem. Soc. Rev.* **2009**, *38*, 1647. (e) Kim, H. N.; Lee, M. H.; Kim, H. J.; Kim, J. S.; Yoon, J. *Chem. Soc. Rev.* **2008**, *37*, 1465.